npj | systems biology and applications

Article

Published in partnership with the Systems Biology Institute

https://doi.org/10.1038/s41540-025-00574-2

# Altered dynamic functional connectivity and reduced higher order information interaction in Parkinson's patients with hyposmia



Sneha Ray[1,2], Navkiran Kalsi[3], Henning Boecker[4], Neeraj Upadhyay[4,6] & Rajanikant Panda[5,6] ✉

Hyposmia, a common non-motor symptom in Parkinson's disease (PD) linked to reduced odor sensitivity, is associated with brain structural and functional changes, but dynamic brain activity and altered regional information exchange remain underexplored, limiting insight into underlying brain states. We selected 15 PD patients with severe hyposmia (PD-SH), 15 PD patients with normal cognition (PD-CN), and 15 healthy controls (HC). Using functional MRI, we assessed the brain's spatiotemporal connectivity (brain-state) alterations, and the brain's capacity for higher-order information exchange (synergy and redundancy). A dynamic brain state with complex-long-range connections was significantly reduced in PD-SH and PD-CN, compared to HC. Brain-states consisting of modular-clusters in sensorimotor and frontal areas occurred more frequently in PD-SH than in PD-CN and HC. Higher-order information flow was reduced in PD patients, with PD-SH showing a greater reduction in synergetic information flow in frontal, insula, and left sensory-motor. These findings suggest potential discriminative biomarkers for PD-SH.

Parkinson's disease (PD) is the second most common neurodegenerative disease, clinically identified by the presence of motor and non-motor symptoms. In early PD, a manifestation of loss of olfactory sensation called "hyposmia" has been reported as a common non-motor symptom. Hyposmia is characterized by reduced odor discrimination, perturbation in odor identification, elevated odor detection threshold, and impaired odor recognition memory[1]. Bohnen and colleagues (2008) postulated that hippocampal dopaminergic denervation and/or dysfunction could lead to olfactory dysfunction in early PD[2]. Alternatively, Lewy body depositions were also associated with hyposmia[3]. Morley and colleagues (2011) demonstrated that hyposmia is linked to executive function deficits, working memory impairment, and psychotic symptoms in PD patients[4]. These studies suggest that olfactory dysfunction in PD is associated with cognitive impairment involving pathological protein aggregations and could be used as a natural lesion model to assess the underlying neural dynamics while considering cognitively normal PD patients as control[4,5].

Resting state functional magnetic resonance imaging (rs-fMRI) studies have revealed distinct functional connectivity (FC) alterations associated with olfactory processing in healthy individuals[6]. In PD patients with hyposmia (PD-SH), static FC analysis highlighted disruptions in thalamo-cortical and associative networks[7] and reduced FC limbic and multimodal cortical regions linked to olfactory processing[8]. Also, data-driven analyses, including ICA and functional covariance mapping, further point to altered connectivity in the precuneus, visual, and olfactory cortices in PD-SH[8,9]. These findings are accompanied by topological alterations that demonstrated reduced small worldness and clustering coefficient suggesting an aberrant reorganization of brain network architecture of PD-SH[8]. However, the majority of these investigations have relied on classical, static FC analyses (i.e., time-averaged) techniques and do not provide information on how the severely decreased brain activity and connectivity alter the spatiotemporal functional repertoire of the brain network and information processing. Furthermore, these static approaches do not fully demonstrate the dynamic and integrative nature of olfactory processing[10,11].

The dynamic functional connectivity (DFC) approach can capture fluctuations in FC over time, thus enabling us to understand how brain regions interact and communicate at different points in time[12]. A recent

[1]Department of Neurosciences, Université de Mons, Mons, Belgium. [2]Department of Psychiatry and Behavioral Sciences, University of California, San Francisco, San Francisco, CA, USA. [3]Jindal School of Psychology & Counselling, O P Jindal Global University, Sonipat, India. [4]Clinical Functional Imaging Lab, Department of Nuclear Medicine, University Hospital Bonn, Bonn, Germany. [5]Department of Neurology, University of California, San Francisco, San Francisco, CA, USA. [6]These authors contributed equally: Neeraj Upadhyay, Rajanikant Panda. ✉e-mail: bk.bme.rajanikant@gmail.com

study using the DFC approach highlighted the multisensory integration mechanisms associated with olfactory loss[13]. These dynamic fluctuations could further be characterized as different brain states recurring over the time capturing the spatiotemporal dynamics at rest. Integration of various brain states (spatiotemporal brain connectivity fluctuations) has been suggested to be associated with higher-order cognitive processes related to multisensory integration[14]. Such multivariate interactions extend beyond simple pairwise correlations and can be more effectively characterized using higher-order information-theoretic measures such as mutual information, transfer entropy, and higher-order information flow[15–17]. In particular, measures of higher-order information flow, i.e., synergy and redundancy can provide valuable insights into the complementary and overlapping information conveyed by different brain regions[18]. These aforementioned dynamic measures may help elucidate the neural substrates underlying multisensory integration, which are often disrupted in olfactory dysfunction associated with PD-SH.

Hence, this study aims to investigate the functional changes in brain dynamics and information flow underlying olfactory dysfunction in PD by comparing PD-SH to those cognitively normal PD (PD-CN) and healthy controls (HC). We implemented the DFC[19], Brain states (pattern)[20] analysis, and higher order information processing using synergy and redundancy[15]. We hypothesize that patients with PD-SH will exhibit distinct brain state dynamics and altered spatiotemporal functional connectivity compared to those without hyposmia (PD-CN). These differences will be reflected in disrupted dynamic functional connectivity patterns and changes in spontaneous higher-order information flow, such as synergy and redundancy. These computational signatures may serve as biomarkers to discriminate PD-SH from PD-CN. We were also interested in associations between the above spatiotemporal dynamic changes and odor identification ability. Finally, we endeavored to determine the optimal features that are potential measures to classify PD-SH from PD-CN.

## Results

Due to vast head movements (>2 mm on rotational and/or translational), three healthy subjects had to be excluded. These three subjects' ICA also showed a higher number of noise components (more than 70% ICs), which led to excluding the subjects from post-processing. Hence, finally, we included 42 subjects (12 HC, 15 PD-CN, and 15 PD-SH) for the post-processing. All the below results were obtained by analyzing this sample. The demographic and behavioral results could be found in the original work[8]. However, an adapted demographic table is provided for further inferences in Table 1.

**Table 1 | Participant demographics**

| | Healthy controls (12) | PD with no/ mild hyposmia (15) | PD with severe hyposmia (15) | *P* values |
|---|---|---|---|---|
| Male/Female | 6/6 | 6/9 | 7/8 | 0.865 |
| Age | 63.3 (5.16) | 64.4(7.2) | 70.7(4.8) | 0.002* |
| Duration | NA | 6.1(3.2) | 5.9(3.7) | 0.8753 |
| ACE-R | 97.3(2.9) | 96.1(3.1) | 94.3(3.4) | 0.043* |
| OSIT-J | 10.5(1.2) | 7.5(1.5) | 1.7(1.1) | < 0.001** |
| Laterality(L/ R/B) | NA | 4/11/0 | 7/7/1 | 0.432 |
| MMSE | 29.3(0.6) | 29.0(1.3) | 29.1(1.1) | 0.990 |
| LEDD | NA | 394.7(277.0) | 455.9(377.8) | 0.616 |
| Hoehn and Yahr stages | NA | 2.0(0.5) | 2.0(0.4) | 1.00 |
| MDSUPDRS-III | NA | 21.2(9.4) | 19.3(7.9) | 0.553 |

*Represent significant differences while ** showed highly significant differences. Data are means ± standard deviation (SD). *PD* Parkinson's disease, *ACE-R* Addenbrooke's Cognitive Examination-Revised, *OSIT-J* Japanese Odor Stick Identification Test, *R* right side predominant, *L* left side predominant, *B* bilateral, *MMSE* mini-mental state examination, *LEDD* levodopa equivalent dose, *MDS-UPDRS* Movement Disorder Society-Sponsored Revision of the Unified Parkinson's Disease Rating Scale, *NA* not applicable.

### Phase based brain dynamic functional connectivity

Both patient groups, the PD-CN (Fig. 1b) and the PD-SH (Fig. 1c), had lower DFC as compared to healthy subjects (Fig. 1a). The group mean DFC was as follows: HC (0.669 ± 0.009), PD-CN (0.662 ± 0.005) and PD-SH (0.661 ± 0.002), with differences in the PD-SH vs HC comparison ($p = 0.003$; $t = 2.94$; Bonferroni-uncorrected) and the PD-CN vs HC; comparison ($p = 0.019$; $t = 2.17$; Bonferroni-uncorrected). There was no difference in the mean DFC between PD-CN vs PD-SH.

### Brain States (Patterns)

We examined the spatio-temporal brain network fluctuation known as brain state (i.e., patterns), which characterizes how brain regions form spatially coordinated functional networks and provide temporal weightage. We found that six brain states are the optimal number for our data based on the iteration approach as proposed by Martínez and colleagues[21]. The six brain states presented in Fig. 2a and b, from which three brain states (Brain State A, Brain State C and Brain State F) have temporal fluctuation (i.e., probability of occurrence) differences between the groups (Fig. 2c).

The brain state A comprises bilateral fronto-parieto-temporal areas, and middle / anterior cingulate areas. The pattern has a higher integrated, long-range (global) association (i.e., frontal with parietal) and a higher rate of occurrence (probability) in healthy individuals compared to PD-CN and PD-SH. The mean occurrence of brain state A in PD-CN (0.20 ± 0.14) was significantly lower compared to HC (0.40 ± 0.22, $p$ and $t$ value = 0.001 and 3.4; Bonferroni corrected). PD-SH (0.20 ± 0.14) had a lower trend of mean occurrences than HC ($p$ and $t$ value = 0.004 and 2.82; Bonferroni-uncorrected). There was no difference between PD-CN vs PD-SH [$p = 0.77$ and $t = -0.77$] in the brain state A (Fig. 2c; Table 2).

The brain state C consists of bilateral sensorimotor and frontal areas. In this state, the pattern has higher modular (segregated) and short-range (local) associations (i.e., sensorimotor-frontal areas). This pattern showed a trend towards a higher probability of occurrence in the patient group compared to healthy individuals, although this trend did not survive Bonferroni correction for multiple comparisons. The PD-CN group exhibited a higher probability of occurrence compared to HC [HC: 0.10 ± 0.07, PD-CN: 0.15 ± 0.04, $p = 0.019$, $t = 2.15$; Bonferroni uncorrected]; The PD-SH group showed an even greater increase in occurrence relative to HC [HC: 0.10 ± 0.07, PD-SH: 0.20 ± 0.10, $p = 0.005$, $t = 2.74$; Bonferroni uncorrected] and also compared to PD-CN [PD-CN: 0.15 ± 0.04, PD-SH: 0.20 ± 0.10, $p = 0.043$, $t = 1.77$; Bonferroni uncorrected] (Fig. 2c; Table 2).

The brain states F consists of bilateral sensorimotor-insula-occipital-hippocampal areas. This pattern has a higher rate of occurrence (probability) in PD-CN patients compared to PD-SH and healthy individuals. The PD-CN was significantly higher than HC [HC: 0.07 ± 0.05, PD-CN: 0.17 ± 0.06, $p = 0.00008$, $t = 4.42$; Bonferroni corrected] and PD-SH [PD-CN: 0.17 ± 0.06, PD-SH: 0.09 ± 0.047, $p = 0.0002$, $t = 3.93$; Bonferroni corrected]. There was no difference between PD-SH and HC groups (Fig. 2c; Table 2).

There was no difference in pattern occurrence between any of the groups (HC, PD-CN, PD-SH) for brain states (pattern) in B, D and E (Fig. 2c; Table 2).

Although there was a non-significant trend toward reduced brain state transitions in healthy controls compared to PD patients ($p > 0.05$), overall transitions between brain states did not show prominent group differences. However, two specific transitions were significantly altered (Bonferroni corrected): the transition from brain state C to state F was significantly lower ($p = 0.0004$, $t = 3.71$, cohen's d = 1.35) in the PD-SH group compared to the PD-CN group, and the transition from Brain State E to State A was significantly lower ($p = 0.0004$, $t = 3.80$, cohen's d = 1.40) in the PD-SH group compared to HC.

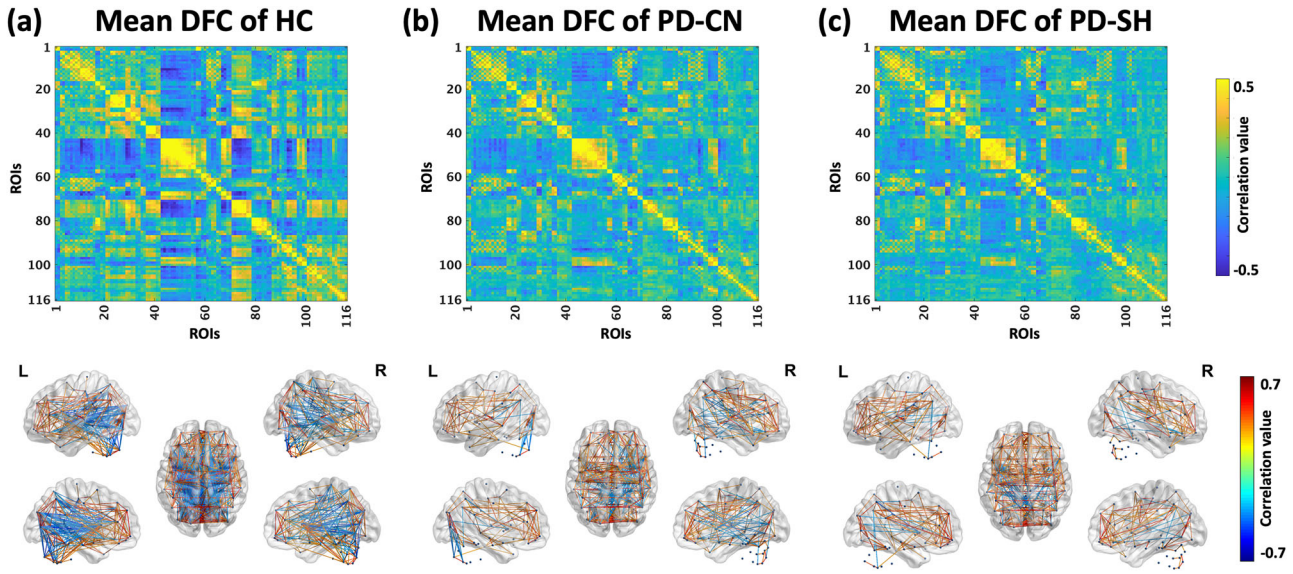


**Fig. 1 | Representation of dynamic functional connectivity (DFC) matrix (upper row) and glass brain visualization (bottom row) for each group.** Group-averaged DFC matrix for **a** healthy controls (HC), **b** Parkinson's with cognitive normal ability (PD-CN), **c** Parkinson with severe hyposmia (PD-SH). The top row displays the group-level average connectivity matrices. Corresponding prominent functiRepresentation of dynamic functional connectivity (DFC) matrix (upper row) and glass brain visualization (bottom row)onal connections (i.e., connections with a strength greater than 0.3 r-values) are visualized in the glass brain representations below each matrix in the bottom row.

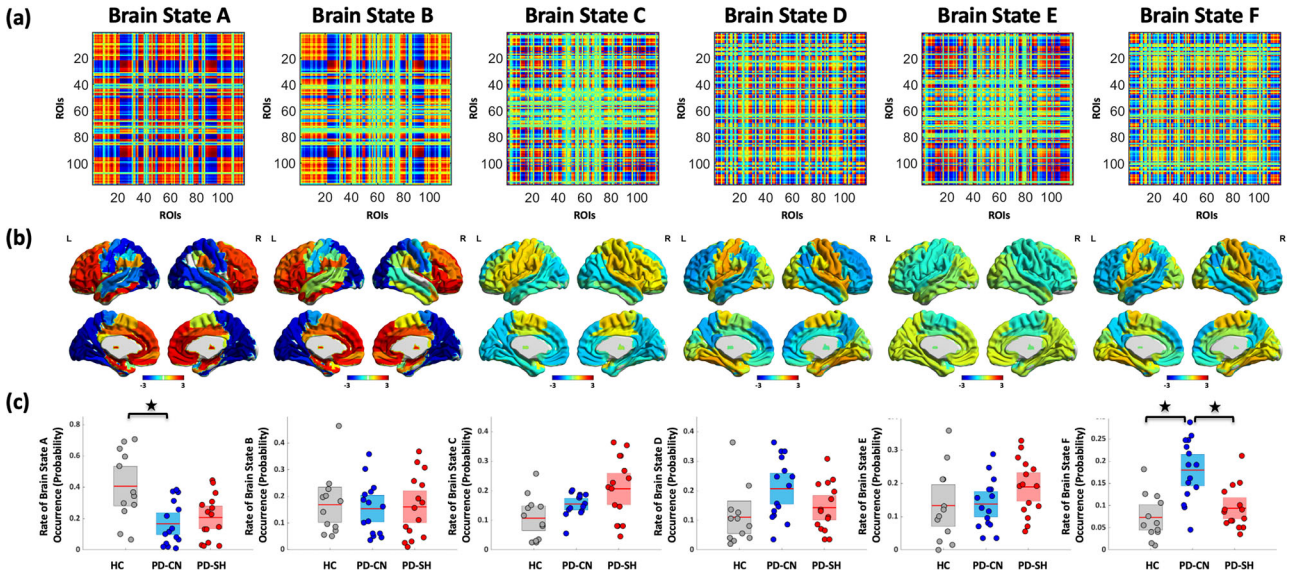


**Fig. 2 | Spatial patterns of brain states matrices (top row), their corresponding glass brain (middle row) and temporal differences between groups (bottom row).** **a** Brain States (patterns) for six different states matrix and **b** their spatial distribution in the glass brain plot using BrainNet viewer. The brain state matrices are computed by taking all the healthy controls (HC), Parkinson's with cognitive normal ability (PD-CN) and Parkinson's with severe hyposmia (PD-SH) dynamic connectivity matrices data. To characterize the different groups, we assess **c** brain state rate of occurrences (probability) for HC, PD-CN & PD-SH. In the bar graph (c) star represents between-group significant difference $P < 0.05$ Bonferroni-uncorrected, and every dot represents the individual subject's mean brain state rate of occurrences values for their corresponding groups.

Finally, to characterize the topological patterns of the brain state matrices, we applied graph-theoretical measures of network segregation (modularity) and integration (participation coefficient). Brain state A exhibited the highest network integration, followed by states D, B, E, and F, while brain state C showed the lowest integration. In contrast, brain states C and D demonstrated the highest network segregation, whereas brain state A had the lowest network segregation.

## Information processing

**Synergy**. We investigated the synergy and redundancy that characterizes higher-order spontaneous brain information interactions, reflecting integrated, complementary information contributed by multiple regions and capturing overlapping or shared information present across those regions, respectively. We noted that whole brain synergy and redundancy were significantly (Bonferroni corrected) lower in PD-CN and PD-SH compared to HC (Fig. 3d). The whole brain mean synergy for HC

**Table 2 | Group difference *p*, *t* and cohens' d values for brain state probability of occurrence and average duration**

| Features | HC VS PD-CN (*p* value; *t* value; cohens'd) | HC VS PD-SH (*p* value; *t* value; cohens' d) | PD-CN VS PD-SH (*p* value; *t* value; cohens' d) |
|---|---|---|---|
| **Probability Occurrence of Brain State** | | | |
| Probability of Brain State A | **0.0011; 3.42; 1.29*** | 0.0046; 2.82; 1.06# | 0.4454; 0.77; 0.28 |
| Probability of Brain State B | 0.6381; 0.35; 0.13 | 0.5668; 0.16; 0.06 | 0.4304; 0.17; 0.06 |
| Probability of Brain State C | 0.0190; 2.15; 0.80# | 0.0055; 2.75; 1.08# | 0.0436; 1.77; 0.64 |
| Probability of Brain State D | 0.0100; 2.48; 0.96 | 0.8224; 0.94; 0.36 | 0.0342; 1.89; 0.69 |
| Probability of Brain State E | 0.4530; 0.11; 0.04 | 0.0760; 1.47; 0.56 | 0.0451; 1.75; 0.64 |
| Probability of Brain State F | **>0.0001; 4.42; 1.74*** | 0.855; 1.08; 0.41 | **0.0002; 3.93; 1.43*** |
| **Average Duration of Brain State** | | | |
| Duration of Brain State A | **0.0008; 3.53; 1.30*** | 0.0849; 1.41; 0.54 | 0.0487; 1.71; 0.62 |
| Duration of Brain State B | 0.4073; 0.23; 0.23 | 0.2682; 0.62; 0.09 | 0.2189; 0.78; 0.28 |
| Duration of Brain State C | 0.0139; 2.33; 0.48 | 0.0286; -1.98; 0.91 | 0.0286; 1.98; 0.72 |
| Duration of Brain State D | 0.1226; 1.19; 0.46 | 0.1003; 1.31; 0.51 | 0.4496; 0.12; 0.04 |
| Duration of Brain State E | 0.0288; 1.99; 0.78 | 0.1413; 1.09; 0.45 | 0.0052; 2.7; 1.005# |
| Duration of Brain State F | 0.0907; 1.37; 0.52 | 0.3359; 0.42; 0.16 | 0.0261; 2.02; 0.74 |

* indicates $p < 0.05$, Bonferroni-corrected for every feature (probability of occurrence and average duration), accounting for 6 brain states and 3 group comparisons (HC vs PD-CN, HC vs PD-SH, and PD-CN vs PD-SH); total comparisons $N = 18$. # indicates a trend of difference (i.e., $p < 0.05$, Bonferroni-uncorrected).

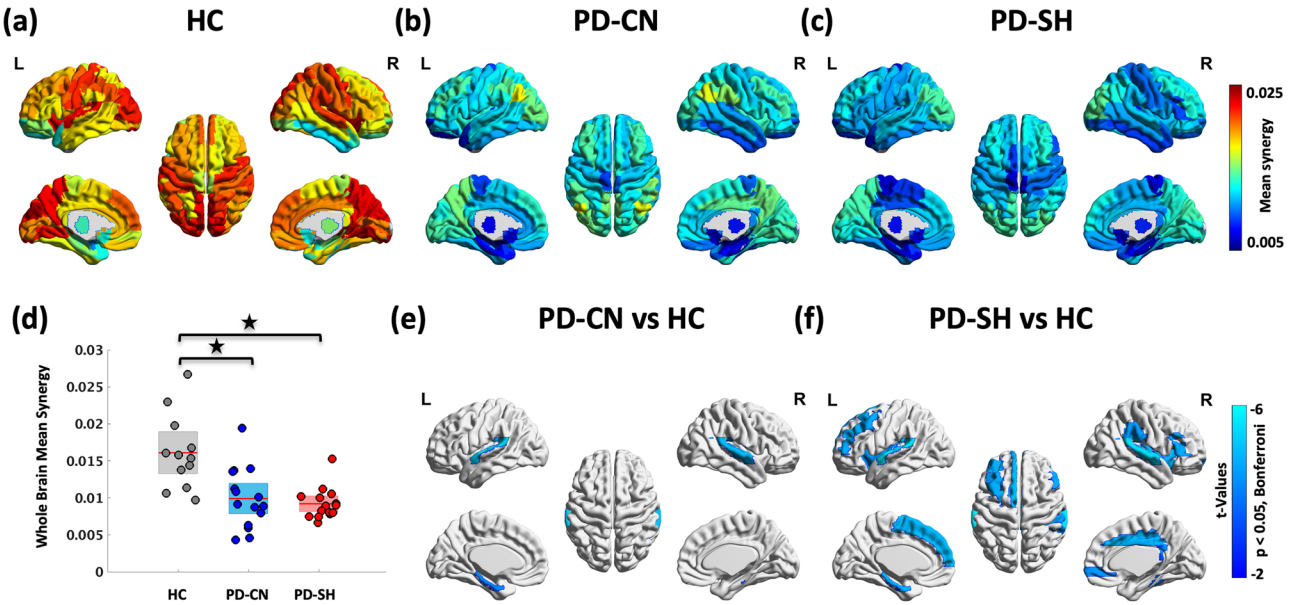


**Fig. 3 | Glass brain representation of mean synergy of each group for each brain region/ROIs (upper row) and between-group differences (bottom row).** Glass brain representation of regional (ROIs level) synergy **a** HC, **b** PD-CN, **c** PD-SH and **d** whole brain mean comparisons of HC, PD-CN and PD-SH, **e** group differences of PD-CN vs HC and **f** group differences of PD-SH vs HC. The group difference for ROI's was computed using a two-sample *t*-test with Bonferroni corrections for multiple comparisons. Negative t (blue to sky color) represents PD-NC and PD-SH to have lower synergy in those regions than HC.

(0.016 ± 0.005), PD-CN (0.01 ± 0.004), and PD-SH (0.009 ± 0.002) [p and t value of PD-SH vs HC = 0.00002 and 4.84; *p* and *t* value of PD-CN vs HC = 0.0007 and 3.54] (Fig. 3D). There was no significant difference in whole brain synergy between PD-CN vs PD-SH [$p = 0.27$ and $t = 0.59$].

We noted PD-SH to have many regions with decreased synergy (Bonferroni corrected) as compared to HC, including bilateral frontal areas (left middle and superior frontal gyrus, right inferior frontal gyrus (triangular) and superior orbitofrontal), left sensorimotor cortex, bilateral superior temporal gyrus, right supramarginal gyrus, bilateral insula, putamen, left parahippocampal and cerebellum (right cerebellum crus-1, 2, 45 & 9, left cerebellum 3 and Vermis 8) (Fig. 3f; Table 3).

Compared to PD-SH, PD-CN has fewer brain regions with reduced synergy compared to HC. The reduced synergy in PD-CN (Bonferroni corrected) was noted at the bilateral superior temporal gyrus, left parahippocampal and cerebellum (right cerebellum crus-1 and bilateral cerebellum 3 and Vermis 45) (Fig. 3e; Table 3). The PD-SH group showed lower mean synergy than PD-CN at the whole brain and brain regional level; however, the difference was not statistically significant.

## Redundancy

We noted significant reduction of (Bonferroni corrected) whole brain redundancy in PD patients (PD-CN and PD-SH) compared to HC (Fig. 4d).

**Table 3 | Group difference *p*, *t* and cohens' d values for brain regions that showed significant difference in synergy or redundancy for any group (i.e., HC vs PD-CN, HC vs PD-SH and PD-CN vs PD-SH)**

| Features | HC vs PD-CN<br>*t* stat; *p* value; cohens'd | HC vs PD-SH<br>*t* stat; *p* value; cohens'd | PD-CN vs PD-SH<br>*t* stat; *p* value; cohens'd |
|---|---|---|---|
| WB Synergy | 3.56; 0.0015; 1.36 | 4.85; >0.0001; 1.80* | 0.60; 0.5570; 0.21 |
| WB Redundancy | 3.89; 0.0006; 1.44 | 4.12; 0.0003; 1.52* | 0.20; 0.8445; 0.07 |
| Syn ROI -L MFG | 1.89; 0.0706; 0.76 | 4.74; >0.0001; 1.81* | 0.56; 0.5829; 0.20 |
| Syn ROI -R IFG Triang | 2.61; 0.0148; 0.10 | 4.71; >0.0001; 1.73* | 1.87; 0.0715; 0.69 |
| Syn ROI -L SMA | 2.47; 0.0208; 0.95 | 4.94; >0.0001; 1.83* | 1.75; 0.0905; 0.64 |
| Syn ROI -L SFG Med | 3.09; 0.0047; 1.19 | 4.93; >0.0001; 1.81* | 0.90; 0.3750; 0.33 |
| Syn ROI -R ORB Sup Med | 3.19; 0.0037; 1.21 | 4.39; 0.0002; 1.63* | 1.06; 0.2960; 0.39 |
| Syn ROI -R REC | 3.74; 0.0009; 1.41 | 4.12; 0.0003; 1.51* | 0.26; 0.7933; 0.10 |
| Syn ROI -L Insula | 2.84; 0.0088; 1.08 | 4.41; 0.0001; 1.62* | 1.10; 0.2797; 0.40 |
| Syn ROI -R Insula | 3.81; 0.0008; 1.43 | 4.88; >0.0001; 1.80* | 1.21; 0.2372; 0.44 |
| Syn ROI -R DCG | 2.05; 0.0512; 0.81 | 4.86; >0.0001; 1.84* | 1.54; 0.1332; 0.56 |
| Syn ROI -R PCG | 2.75; 0.0108; 1.08 | 4.40; 0.0001; 1.64* | 0.15; 0.8811; 0.05 |
| Syn ROI -L Parahippocampal | 4.13; 0.0003; 1.55* | 4.84; >0.0001; 1.79* | 0.75; 0.4596; 0.27 |
| Syn ROI -R SMG | 2.02; 0.0544; 0.79 | 4.52; 0.0001; 1.70* | 1.68; 0.1036; 0.61 |
| Syn ROI -R Putamen | 3.30; 0.0028; 1.26 | 4.71; >0.0001; 1.74* | 0.10; 0.3272; 0.36 |
| Syn ROI -L STG | 5.37; >0.0001; 2.03* | 5.76; >0.0001; 2.16* | 0.01; 0.9955; 0.01 |
| Syn ROI -R STG | 5.01; >0.0001; 1.91* | 5.60; >0.0001; 2.07* | 0.70; 0.4905; 0.26 |
| Syn ROI -R CRBL Crus1 | 4.05; 0.0004; 1.50* | 4.25; 0.0002; 1.56* | 0.10; 0.9222; 0.04 |
| Syn ROI -R CRBL Crus2 | 3.54; 0.0016; 1.33 | 4.25; 0.0002; 1.56* | 0.53; 0.5998; 0.19 |
| Syn ROI -L CRBL3 | 5.03; >0.0001; 1.87* | 4.50; 0.0001; 1.69* | 0.33; 0.7474; 0.12 |
| Syn ROI -R CRBL45 | 3.42; 0.0021; 1.33 | 4.40; 0.0001; 1.66* | 0.05; 0.9572; 0.02 |
| Syn ROI -R CRBL9 | 3.34; 0.0026; 1.25 | 4.40; 0.00017; 1.62* | 1.10; 0.2816; 0.40 |
| Syn ROI -R CRBL8 | 2.35; 0.0271; 0.90 | 4.40; 0.0001; 1.66* | 1.50; 0.1434; 0.55 |
| Red ROI - L Parahippocampal | 4.79; >0.0001; 1.79* | 6.49; >0.0001; 2.38* | 2.13; 0.0418; 0.78 |
| Red ROI -R PoCG | 2.30; 0.0302; 0.87 | 4.10; 0.0003; 1.50* | 2.03; 0.0516; 0.74 |
| Red ROI -R STG | 4.66; >0.0001; 1.77* | 4.89; >0.0001; 1.82* | 0.48; 0.6345; 0.18 |
| Red ROI -R CRBL Crus1 | 4.17; 0.0003; 1.53* | 4.26; 0.0002; 1.55* | 0.02; 0.9825; 0.01 |
| Red ROI -R CRBL9 | 3.98; 0.0005; 1.46 | 4.15; 0.0003; 1.51* | 0.30; 0.7645; 0.11 |
| Red ROI -Vermis7 | 3.89; 0.0007; 1.44 | 4.77; >0.0001; 1.74* | 1.23; 0.2300; 0.45 |

* indicates $p < 0.05$, Bonferroni-corrected.

The whole brain mean redundancy for HC (0.03 ± 0.014), PD-CN (0.013 ± 0.006), and PD-SH (0.013 ± 0.005) [p and t value of PD-SH vs HC = 0.0001 and 4.11; *p* and t value of PD-CN vs HC = 0.0003 and 3.89] (Fig. 4d). There was no significant difference in whole brain synergy between PD-CN vs PD-SH [$p = 0.42$ and $t = 0.19$].

We noted PD-SH to have many regions of decreased redundancy compared to HC (Bonferroni corrected), including bilateral parahippocampal, right superior temporal gyrus and postcentral gyrus, and cerebellum (right crus-1 and 9 and vermis 7) (Fig. 4f; Table 3). The PD-CN shows similar brain region redundancy differences (Bonferroni corrected) including bilateral parahippocampal, right superior temporal gyrus, and cerebellum (right crus-1 and bilateral cerebellum 3) (Fig. 4e; Table 3). There was no difference in whole brain redundancy as well as regional level redundancy between PD-SH and PD-CN groups.

### Feature Ranking and Classification

To identify potential neurophysiological biomarkers differentiating PD-SH from PD-CN, we employed a two-step machine learning approach combining supervised classification and feature ranking. The feature selection algorithm retained the top 20% of features by ranking them and selecting those whose scores were above the overall mean of all feature ranking F-test scores, corresponding to eight key predictors. These included: probability of brain state C, transition probability from state C to F, mean duration of brain state C, synergy of posterior cingulate gyrus, supramarginal gyrus, superior temporal gyrus, and superior frontal gyrus, and a redundancy measure from parahippocampal gyrus (See Fig. 5).

Our different classifiers results highlight a well-balanced and robust model performance (Table 4). The Gaussian Naive Bayes (GaussianNB) model demonstrated strong discriminative performance, achieving an AUC of 0.93% and an accuracy of 91%. Sensitivity was 86.6%, indicating effective identification of PD-SH cases, while specificity was 88.4%, reflecting accurate classification of PD-CN cases (see Fig. 6, Table 4).

### Behavioral correlation

We noted significant positive correlations (i.e., partial Pearson correlation controlling for age and cognitive score (ACE-R)) between Japanese Odor Stick Identification with synergy of somatosensory area ($r = 0.33$, $p = 0.04$, 95%CI: [0.02, 0.58]), Parahippocampus ($r = 0.30$, $p = 0.05$, 95%CI: [−0.0, 0.57]), and redundancy in Parahippocampus gyrus ($r = 0.46$, $p = 0.002$, 95% CI: [0.17, 0.68]). In contrast, the rate of occurrences of brain state C was negatively correlated with odor identification performance ($r = -0.32$, $p = 0.04$, 95%CI: [−0.58, −0.02]).

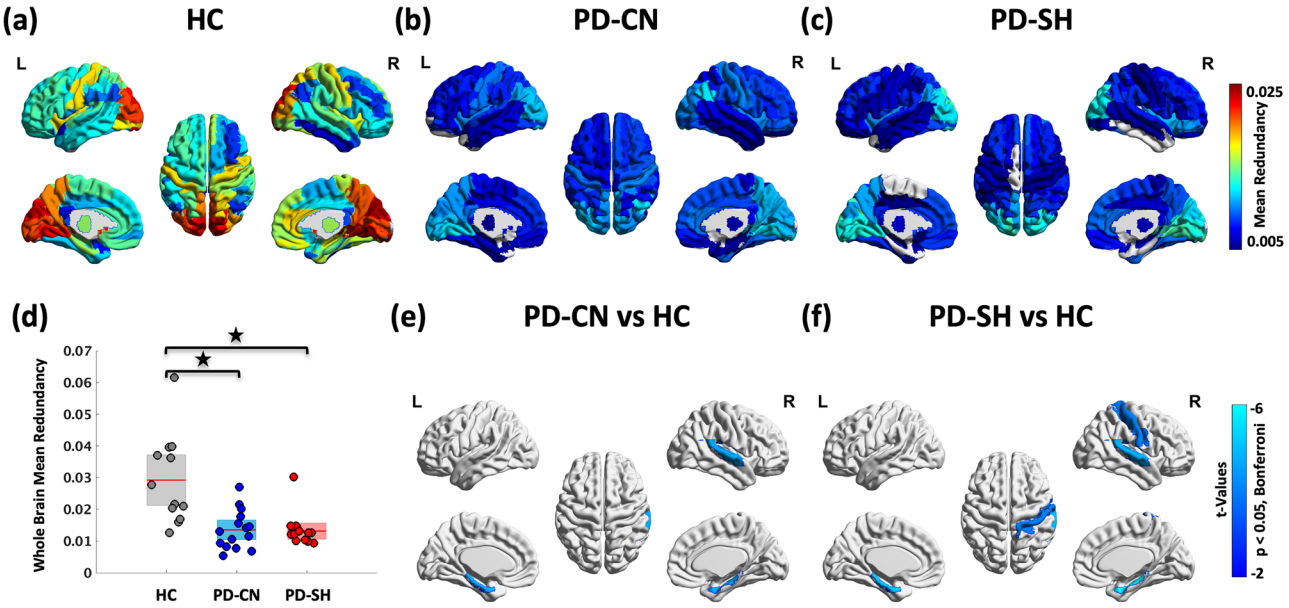


**Fig. 4 | Glass brain representation of mean redundancy of each group for each brain region/ROIs (upper row) and between-group differences (bottom row).** Glass brain representation of regional (ROIs level) redundancy **a** Healthy Control (HC), **b** PD with cognitive normal ability (PD-CN), **c** PD with severe hyposmia (PD-SH and **d** whole brain mean comparisons of HC, PD-CN and PD-SH, **e** group differences of HC > PD-CN and **f** group differences of HC > PD-SH. The between-group difference for ROI's was computed using a two-sample t-test with Bonferroni corrections for multiple comparisons. Negative t (blue to sky color) represents PD-CN and PD-SH to have lower redundancy in respective brain regions than HC.

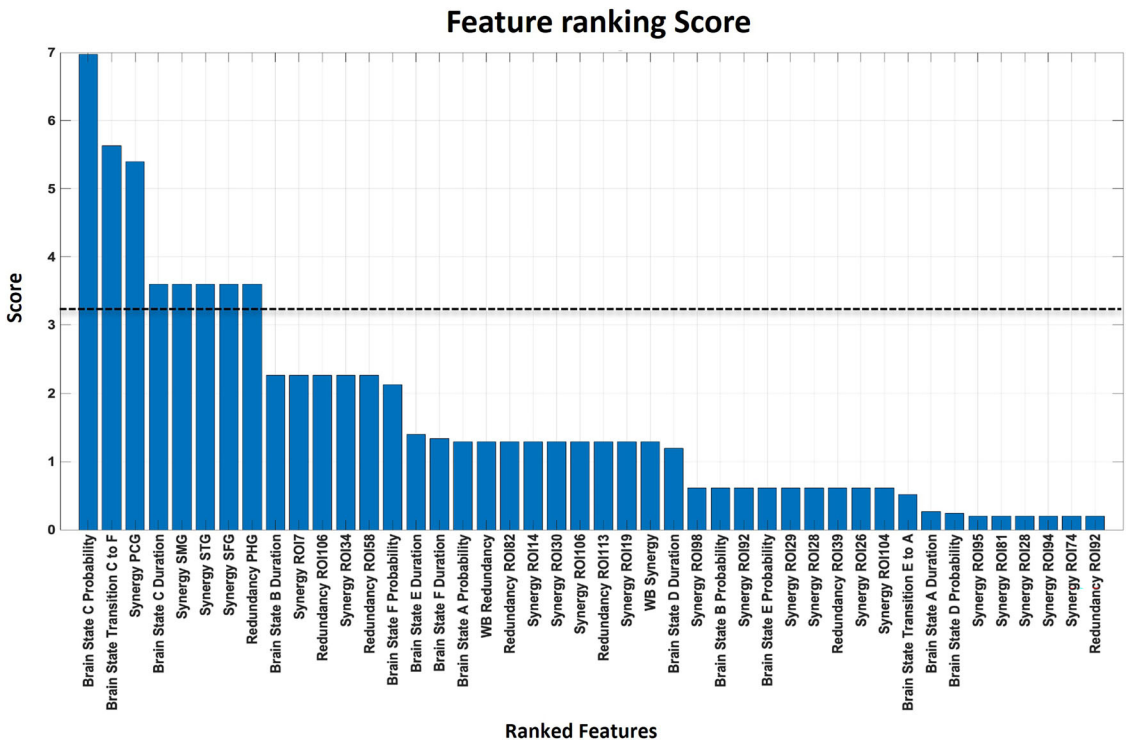


**Fig. 5 | Feature Ranking F-test scores, which shows dominate features.** The top 20% ranked features: included: probability of brain state C, transition probability from state C to F, mean duration of brain state C, synergy of posterior cingulate gyrus, supramarginal gyrus, superior temporal gyrus, and superior frontal gyrus, and a redundancy measure from Parahippocampus gyrus.

## Discussion

In this study, we implemented DFC based approaches to capture altered brain states as well as higher-order information flow to reveal the underlying neural substrates of hyposmia in PD patients compared to PD-CN and HC. The DFC and probability of appearance of a brain state A that consists of complex, long range-global connections composed of frontal-parietal-temporal and anterior cingulate areas was significantly decreased in the patients' group (both PD-SH and PD-CN) compared to HC. A notable finding of our study is that the brain state C, which has prominent modular-local clusters consisting of sensorimotor and frontal areas, had increased

rate of occurrence in the patient groups compared to HC, as well as in the PD-SH group compared to the PD-CN group, suggesting increased segregation. While looking at the transition, we observed that brain state C to F transition significantly lower in the PD-SH compared to PD-CN. Feature selection classification as well as behavioral correlation between the odor identification scores shows brain state C as a prominent measure that could discriminate the PD-SH from PD-CN. Additionally, the higher-order information (i.e., synergy and redundancy) was significantly reduced in the bilateral superior temporal cortex, parahippocampus, and cerebellum areas in the PD patients (both PD-CN and PD-SH). Though no significant differences were found between PD-SH and PD-CN globally, feature selection and classification analysis showed synergy in posterior cingulate gyrus as an important measure for discriminating PD-SH from PD-CN. In addition, positive associations of synergy scores in somatosensory and parahippocampal regions with odor identification scores suggest an involvement of synergistic approach in olfactory processing in PD-SH.

Functional MRI studies have revealed that FC across brain regions fluctuates with distinct spatial patterns across time, referred to as 'brain states'. These 'brain states' consist of predominantly two types of patterns, one is complex-long-range pattern, the other short-range modular connections, both globally as well as locally[19,22]. In healthy individuals, the complex-long range brain state (denoted as brain state A), consisting of many functional areas, has a higher appearance (dwell time) during awake conscious states or while performing cognitive activities[23]. In our study, we observed a significant decrease in brain state A in both PD-SH and PD-CN compared to HC, suggesting a reduction in complex, long-range interactions due to degenerative processes such as lewy body accumulation. In contrast, the brain states which consist of modular/clusters with fewer brain regions (i.e., simple pattern; denoted as brain states C) have less probability of occurrence in HC. Fiorenzato et al. (2019) have shown an increase in dwell time (rate of occurrence) in cognitively impaired PD patients[23]. According to them, the cognitive decline in memory might be associated with the existence of increased dwell time among the segregated brain states in addition to reduced transition of brain states. Similar to this, the increased dwell time of brain state C in our study involving sensorimotor modulation deviated from the PD-CN. The local clusters could be representative of the increased occurrence of segregation state in the sensorimotor and frontal regions. Such increased segregation might affect the olfactory processes which is known as an integrative process[7,13]. Overall, our findings of decreased rate of occurrence for complex pattern (brain state A) and increased rate of occurrence of simpler-modular brain state (brain state C) in PD validate the observations of previous studies[23–25]. Here we have demonstrated that the complex-long range interactions are decreased in PD-SH and in PD-CN, however, the simpler pattern is dominant in PD-SH compared to PD-CN, and associated with the degree of odor identification measured through behavioral tests. Furthermore, we observed brain state C as a prominent feature that discriminates PD-SH from PD-CN. Hence, the duration of brain state C (i.e., simpler modular connectivity pattern) as well as transition from brain state C to F properties may play an important role in early discrimination of PD-SH which need to be validated in a larger cohort in early stages of PD.

In addition to the connectivity approach, information theory helps to characterize the complexity of neural signals and how signals from different brain regions influence each other. Recent advances have revealed that spontaneous brain activity exhibits a unique spatiotemporal causal structure of information flow across regions[15–17,26,27]. Some regions integrate information synergistically, while others carry redundant information, often similar to neighboring regions[15–17,26,27]. This balance between synergy and redundancy is maintained during resting and cognitive states. Olfaction has been suggested as a multisensory integrative process which might need

**Table 4 | Classification performance for PD-CN vs PD-SH (i.e., AUC, Accuracy, Sensitivity (true positive ration) and Specificity (true negative ration)) for various model - Gaussian Naive Bayes (GaussianNB), Multi-Layer Perceptron (MLP), Random Forest, Linear SVM, Logistic Regression**

| Classifier | AUC | Accuracy (in %) | Sensitivity (TPR) (in %) | Specificity (TNR) (in %) |
|---|---|---|---|---|
| Gaussian NB | 0.93 | 87.8 | 86.6 | 88.4 |
| Multi-Layer Perceptron (MLP) | 0.91 | 87.8 | 80.0 | 92.3 |
| Random Forest | 0.89 | 78.04 | 60.0 | 88.4 |
| Linear SVM | 0.88 | 87.8 | 73.3 | 96.1 |
| Logistic Regression | 0.88 | 82.9 | 60.0 | 96.1 |

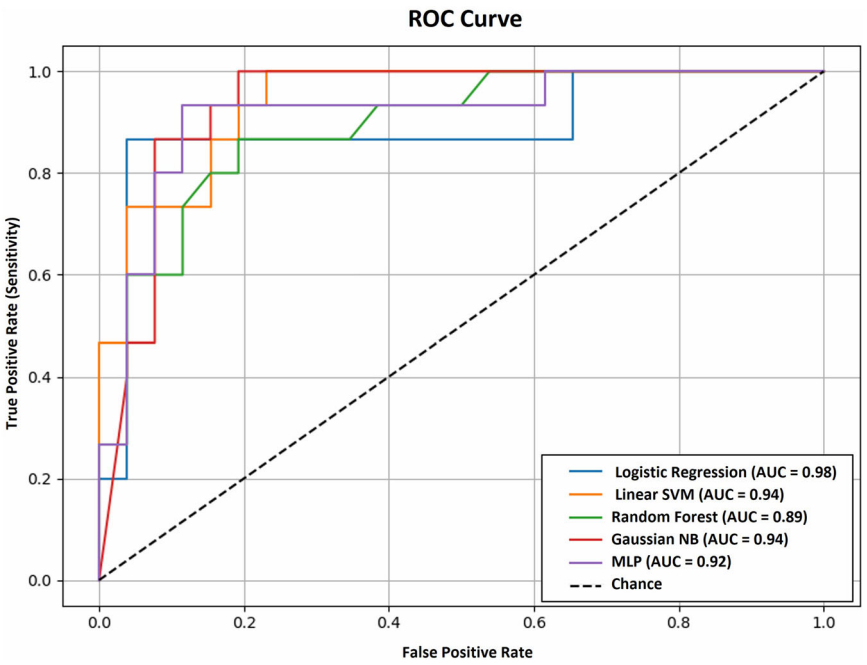


**Fig. 6 | ROC curve for all the classifiers to distinguish PD-SH from PD-CN.** ROC curves for logistic regression (blue), linear SVM (orange), random forest (green), gaussian NB (red) and MLP (purple). Where we observed logistic regression show high sensitivity in discriminating PD-SH from PD-CN.

higher synergy between regions to integrate the information[13]. Our cohort with PD showed reduced synergy as well as redundancy that might be due to a change in the balance of differentiation and integration towards more desynchronized arrangements. Reduced synergy in both PD cohorts might be due to morphological changes (i.e., pathological protein aggregation) leading to altered synergy as well as reduced redundancy due to unavailability of a certain network or circuit or receptors to transfer the information. Although, higher order information processing (i.e., Synergy and redundant information flow) did not discriminate between the PD-SH from PD-CN, we noted PD-SH to have many regions with lower Synergetic information flow, including bilateral frontal, insular, somatosensory, and parahippocampal regions—areas integral to olfactory cognition[28]. This suggests that not only disruption in brain connectivity and spatiotemporal properties, but also alteration of information flow in the brain hub regions could be associated with olfactory dysfunctions in PD. The synergetic information flow reductions were not only spatially specific but behaviorally relevant: synergy in the somatosensory and parahippocampal cortices positively correlated with olfactory performance, indicating that diminished integrative capacity in these regions contributes directly to perceptual deficits.

Iannilli et al. (2017) showed decreased EEG global field power in frontoparietal and central electrodes in PD with olfactory dysfunction[29]. Yoneyama et al. (2018) showed decreased FC in the frontal, amygdala, inferior parietal lobule, lingual gyrus, and fusiform gyrus in PD-SH[8]. Moreover, Wang et al. (2022) demonstrated decreased functional covariance connectivity along with the gray and white matter in the insula and olfactory-related brain regions in PD-SH[9]. Our findings provide a mechanistic explanation for the previously reported reductions in frontoparietal connectivity, EEG power, and regional gray matter changes in PD-SH, indicating that these alterations may result from disrupted spatiotemporal brain dynamics and impaired higher-order information integration. Reduction synergy in limbic, frontal, insular, parahippocampus, superior temporal, and cerebellum regions is in accordance with the above evidence of disrupted olfactory and cognitive processing in PD. These cortical and mesolimbic regions form key hubs of multisensory integration, memory encoding, and executive control, and their diminished synergistic information flow suggests impaired capacity for distributed, cooperative computation. This network-level dysfunction surpasses localized structural or static functional changes, indicating a breakdown in dynamic, higher-order information integration. Such disruption is likely driven by region-specific vulnerability to α-synuclein aggregation, contributing to heterogeneous cognitive phenotypes observed in PD. Additionally, network segregation as observed in modular state C or transition from brain state C to F could be used not only to classify PD-SH and PD-CN, but also to model clinical prognosis and, potentially, treatment effects in larger cohorts in early stages of PD.

Despite the demonstration of significant alterations in dynamic connectivity and information theory measures, the study suffers a lack of power and generalizability due to small sample size. Therefore, future studies with a larger sample are warranted for validation of the reported results. We have to acknowledge as well that no GSR was performed, and this could potentially lead to contamination of connectivity estimates in phase-based analyses, affecting the results. An ICA-based denoising approach, as used in our study, is also capable of removing physiological noise. Five different algorithms were used for feature selection and classification, reporting valuable findings: however, due to the small sample size overfitting has to be considered as a possible source of bias. Finally, implementation of combined functional (task-based or resting fMRI) and structural (gray matter or DTI connectivity matrix) data to explore spatio-temporal dynamic alterations could provide a more biologically informed understanding of olfactory dysfunction in patients with PD.

In conclusion, this study shows reduced dynamic FC in different brain states in PD compared to healthy individuals. Importantly, we report that the brain states specific to bilateral sensorimotor-insula-occipital-hippocampal areas are altered in PD-SH compared to PD-CN and HC. Such disruption of spatiotemporal FC and higher-order information exchange in PD patients, which further worsens in PD patients with hyposmia, could help discriminate PD subgroups in early stages of the disease. PD patients with hyposmia have a higher modular-local pattern (brain state C) appearance and show a decrease of synergy in the frontal, insula, and postcentral gyrus compared to PD-CN and HC. Thus indicating overall perturbation of multisensory integration and could be used as functional markers of hyposmia in PD. These data open new perspectives for further studies on higher-order information exchange in larger early-stage PD cohorts.

## Methods

We extracted MRI data of PD-SH, PD-CN, and HC from the OpenfMRI database, which is dedicated to developing biomarkers for Parkinson's disease in Japan (https://www.openfmri.org/dataset/ds000245/)[8]. The accession number is ds000245.

### Participants

Structural (i.e., T1 weighted) and resting state functional MRI data of 45 subjects were selected, including 15 (7 males and 8 females; 70.7 ± 4.8 years) PD-SH and 15 (6 males and 9 females; 64.4 ± 7.2 years) PD-CN. For the comparison, we have selected 15 (7 males and 8 females; 63.3 ± 5.2 years) HC from the same database. For detailed demographic information, please refer to the original article[8]. The patients were diagnosed as per the United Kingdom Brain Bank criteria and were between 55-75 years of age[20] and were in the Stages I–III according to Hoehn and Yahr (HY) scale[30]. The patients did not report any history of other neurological or psychiatric diseases and showed no family history of PD. Focal deep white matter abnormalities >Grade 2 based on the Fazekas classification system were excluded[31]. Also, PD patients with dominant tremors were excluded to minimize the chance of motion artefacts. A written informed consent was obtained from each participant after explaining the study design. The study follows the Helsinki criteria and was approved by the ethical Committee of Nagoya University Graduate School of Medicine.

### Behavioral assessment

For assessing the odor identification ability of the participants, the Japanese Odor Stick Identification Test (OSIT-J; Daiichi Yakuhin, Co., Ltd., Tokyo, Japan)[32] was conducted. The OSIT-J consists of 12 different odorants familiar to the Japanese and is commonly used for assessing olfactory function in PD patients. In addition, the cognitive functions were assessed using Addenbrooke's Cognitive Examination Scale (Addenbrooke's Cognitive Examination Revised, ACE-R)[33]. The ACE-R assesses six distinct cognitive domains (orientation, memory, attention, language, verbal fluency and visuospatial ability) and can be used to diagnose dementia subtype in PD patients[34]. Exclusion criteria were OSIT-J scores > 4, ACE-R scores ≤ 88, and psychotic behavior, depressed mood, hallucinations, dopamine dysregulation syndrome, anxiety, and apathy based on the Japanese version of the Unified Parkinson's Disease Rating Scale (MDS-UPDRS)[35] as mentioned by Yoneyama et al.[8]

### MRI data selection

MRI data were acquired using a 3.0 T MRI scanner (Siemens, Erlangen, Germany) with a 32-channel head coil at the Brain and Mind Research Center, University of Nagoya, Japan. The high-resolution anatomical (i.e., structural) T1-weighted 3D gradient echo sequences images were acquired with a repetition time (TR) = 2500 ms, echo time (TE) = 2.48 ms, slice thickness = 1 mm, 192 sagittal slices, field of view (FOV) = 256 × 256 $mm^2$, and matrix dimension = 256 × 256. The total scan time of T1-weighted images was 5.49 minutes. The resting-state (task free) functional MRI data was acquired using an EPI gradient echo sequence with the following

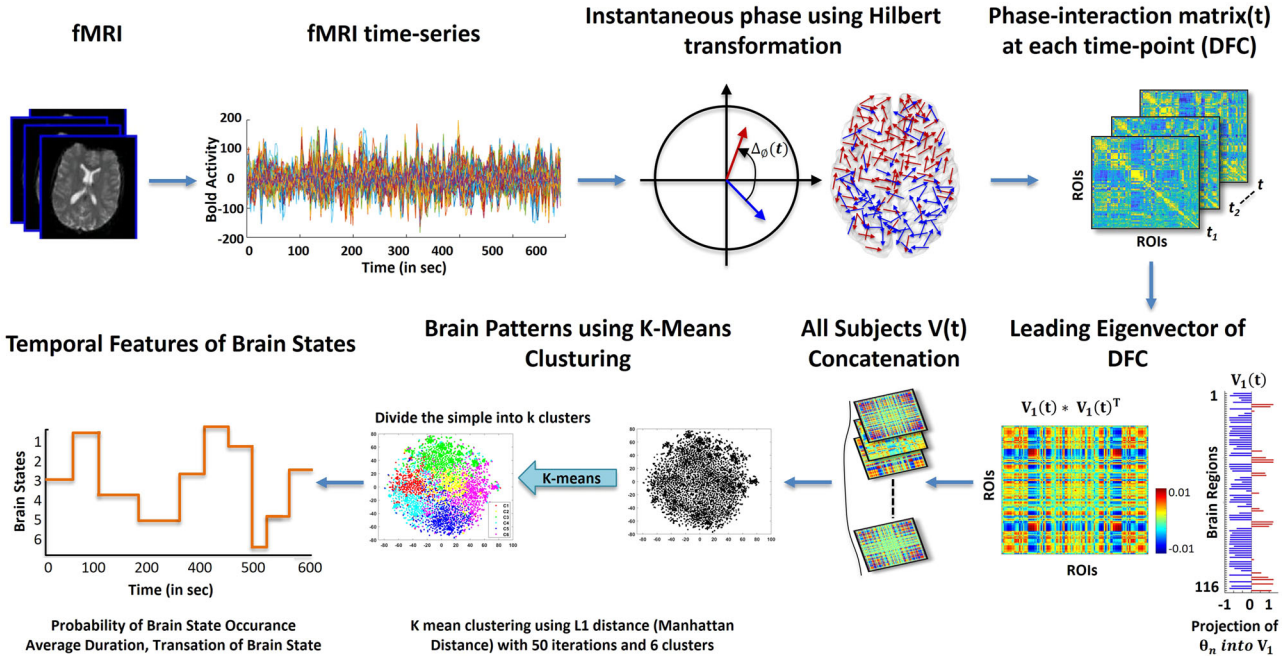


**Fig. 7 | Schematic diagram of dynamic functional connectivity and brain state analysis.** BOLD time series were first extracted for each region of interest. Phase-based dynamic functional connectivity (DFC) was computed by generating instantaneous connectivity matrices at each time point. The leading eigenvector of each matrix was then derived, representing the dominant connectivity pattern at that moment. These eigenvectors were concatenated across all subjects to form a unified dataset. K-means clustering using Manhattan (L1) distance and 50 iterations was applied to identify recurring connectivity configurations, termed brain states. Finally, the temporal characteristics of these brain states, including their probability of occurrence, were quantified.

parameters: TR = 2.5 s, TE = 30 ms, layer spacing = 0.5 mm, 39 transverse slices, 3 mm of thickness, FOV = 192 mm, matrix size = 64 × 64, and flip angle (FA) = 80 degrees. The total rs-fMRI image scanning time was 8 minutes with the eye closed while awake. Patients were in the "ON" medication state when MRI data were acquired.

## Data analysis

Preprocessing of resting fMRI data was performed using MELODIC (Multivariate Exploratory Linear Optimized Decomposition into Independent Components) version 3.14, which is part of FSL (FMRIB's Software Library, http://fsl.fmrib.ox.ac.uk/fsl) with the following steps: the first two functional images were discarded to reduce scanner inhomogeneity, motion correction using MCFLIRT, non-brain tissue was removed using BET, the intensity was normalized, temporal high pass filtering (100 s), spatial smoothing was applied using a 5 mm FWHM Gaussian kernel, and finally rigid-body registration and single-session ICA with automatic dimensionality reduction was applied. Data showing translation motion (>2 mm) between the volumes were excluded. After the ICA computation for each subject's data, noise components (e.g., head movement, metal, and physiological noise artifacts) were manually regressed out for each subject. FSLeyes in MELODIC mode was used to identify the Independent Components (ICs) into "good" for cerebral signal, "bad" for noise artifacts, and "unknown" for ambiguous components at the single-subject level. Each component was evaluated based on the spatial map, spatial map time series and the temporal power spectrum of time series[36,37]. Then, FIX was applied with default parameters to remove bad and lesion-driven artifacts components (FIX, https://fsl.fmrib.ox.ac.uk/fsl/fslwiki/FIX)[36]. Hand classified data driven ICA components robustly removes physiological and structured noises from the rsfMRI data[38], therefore, we did not implement global signal regression, which might introduce spurious anticorrelations and further reduce the sensitivity[39]. Moreover, GSR is clinically and topologically relevant[40,41]. Subsequently, we used an Anatomical Automatic Labeling (AAL2)[42] atlas for parcellations to obtain the Blood Oxygenation Level Dependent (BOLD) time series of the 116 cortical, subcortical, and cerebellum brain areas in each individual's native EPI space[43]. The clean functional data were co-registered to the T1-weighted structural image using FLIRT. The T1-weighted image was co-registered to the standard MNI space using FLIRT (12 DOF) and FNIRT[44]. This transformation matrix was inverted and applied to warp the atlas from MNI space to the single-subject functional data. Finally, the time series for each of the 116 brain areas was extracted using custom-made Matlab scripts[45].

## Dynamic functional connectivity

To assess brain spatiotemporal connectivity properties, we computed the temporal fluctuations of FC over time using the DFC approach. This approach has been used in many studies to understand the functional alterations in the pathophysiology of PD[23,46–48]. However, there are no studies yet using DFC approaches on PD with hyposmia. We use these measures to evaluate the level of regional brain interaction (i.e., synchronicity) and to quantify the spatiotemporal network dynamics.

We calculated the DFC matrices by applying instantaneous phase synchronization to the signal at each time point. Prior to computing the DFC, the BOLD time series were filtered using a band-pass filter in the range of 0.03–0.08 Hz. Then, we performed the Hilbert transform to estimate the instantaneous phases, $\phi_j(t)$ for each region 'j', which obtain the analytic representation of the BOLD time series[49]. The analytic signal, s(t), represents a rotating vector with an instantaneous phase, $\phi(t)$, and an instantaneous amplitude, A(t), represented as follows:

$$s(t) = A(t)\cos\left(\phi(t)\right) \quad (1)$$

Synchronization between brain regions was characterized by the cosine of the phase difference modulus. At each time point, the phase difference $P_{ij}(t)$ between two regions j and k was calculated[50–52]. First to understand brain synchronization level, we computed the mean functional connectivity matrix by taking the average over all time point connectivity matrix and the whole brain DFC was computed taking the average across all brain regions connectivity.

### Brain states

The brain state (i.e., patterns) represents the spatio-temporal brain network fluctuation in a specific state (e.g., resting state), which characterizes how brain regions form spatially coordinated functional networks and provide temporal weightage. The three-dimensional phase-based DFC tensor with size NxNxT (N = ROIs = 116, T=time point = 198) is used to assess the brain state. To characterize the evolution of the DFC matrix over time, first, we compute the leading eigenvector to reduce the dimensionality of each three-dimensional phase-based DFC for each subject by employing a leading Eigenvector Dynamics method Analysis (LEiDA)[21,53]. The resulting leading eigenvector $V_1(t)$ is a one-dimensional (i.e., Nx1; N=ROIs) vector for each DFC tensor (i.e., NxN phase-locking matrix at time t) (see Fig. 7).

To identify recurrent phase-connectivity patterns (named brain states), we used clustering analysis on all the leading eigenvectors $V_1(t)$ across time points and all the subjects (i.e., 116 × 42 = 4872 leading eigenvectors). Then, we use the k-means clustering algorithm that was applied to the concatenated matrix using the L1 distance (a.k.a. "Manhattan distance") as implemented in MATLAB (MathWorks Inc.)[19,53,54]. The clustering approach was applied 50 times each to reduce the local minima using a random initialization of centroid positions. The resultant k-mean clustering provides k number of patterns ($V_C$; called brain states) and labels for each time-points. Since the optimal number of functional networks to consider remains an open question, we ran the k-means clustering algorithm with k ranging from 3 to 10. We took the optimal k values by considering the highest coverage of brain states[53,54]. Finally, we compute the probability of occurrence for each brain state over whole time period of BOLD signal (see Fig. 7). To characterize the topological patterns of the brain state matrices, we applied graph-theoretical measures of network segregation commuted using modularity approach and network integration using participation coefficient[55] as implemented in the Brain Connectivity (BCT)[56] Toolbox.

We computed brain state using LEiDA because unlike classical amplitude-based sliding-window correlation, which relies on arbitrary window lengths and often suffers from limited temporal resolution, LEiDA provides a windowless, data-driven approach that preserves fine-grained phase relationships and allows the identification of recurring whole-brain phase-locking states. This method has been successfully applied in several clinical and healthy populations to characterize alterations in brain state dynamics[53,54]. While non-negative tensor factorization methods offer complementary insights, they typically require higher-dimensional data representations (e.g., multi-subject tensors) and a priori spatial pattern[57,58]. In contrast, the LEiDA framework allowed us to extract robust and interpretable spatiotemporal brain state dynamics at the subject level[53,54].

### Information processing

The information processing measure was used to examine the degree to which two or more variables encode information with another variable, considering it a target variable[59]. FC analysis is limited to pairwise interactions and higher-order interactions across more than two variables leading to the concept of multivariate transfer entropy, synergy, and redundancy, which are considered to be the key aspects of studying neural dynamics[59].

### Synergy and redundancy

The synergy and redundancy represent the higher-order interaction for information flow across brain regions[15–17]. Synergy quantifies how brain regions mutually influence each other's activity over time: that is, the integration of information between those regions whereas redundancy quantifies the common information shared between pairs or regions[15–17].

We compute the synergy and redundancy from higher-order O-Information as proposed by Gatica et al.[15]. O-Information represents for higher-order information denoted as $\Omega(X^n)$ for interdependencies variables (X) from a specific no of modules (M = 116; no of brain regions). The O-Information "$\Omega(X^n$ is a real value measure and it's sign discriminate between synergistic and redundant components (If $\Omega(X^n) < 0$ it corresponds to synergy-dominated interdependencies; whereas $\Omega(X^n) > 0$, represent the redundancy-dominated interdependencies values). The O-Information we assessed by quantify the strength of multivariate correlation for a set of n random variables for each ROIs as follows:

$$\Omega(X_n) = \mathrm{TC}(\mathrm{X_n}) - \mathrm{DTC}(\mathrm{X_n}) \quad (2)$$

TC is the total correlation, and DTC corresponds to the dual total correlation, which are basically non-negative generalizations of mutual information[15]. Here, in this study the redundancy-and synergy-dominated systems was computed with $n = 3$ ($n$= number of interaction order/triplets that include to assess strength interdependencies)[15].

### Statistics and classification

Two-sample one-tailed t-tests were used to calculate the group difference (i.e., PD-CN vs HC, PD-SH vs HC, PD-CN vs PD-SH) for DFC, brain states rate of occurrences measures, synergy, and redundancy. To assess stronger group differences, Bonferroni-corrected multiple comparisons were performed separately for each feature (i.e., probability of occurrence, average duration, and brain state transitions). For probability of occurrence and average duration, multiple comparison correction was applied across 6 brain states and 3 group comparisons (HC vs PD-CN, HC vs PD-SH, and PD-CN vs PD-SH), totaling 18 comparisons. The brain regional measures for synergy and redundancy were assessed using two-sample one-tailed t-tests with multiple comparisons with Bonferroni corrections < 0.05 accounting the number of brain regions ($N = 116$). Brain regions' significant changes are visualized using the BrainNet viewer.

The whole Brain dynamics (DFC, brain state, synergy, and redundancy) and regional changes of synergy and redundancy that revealed significant differences between patient groups and healthy individuals, were correlated with behavioral assessments of cognitive and odor identification abilities (OSIT-J score) using partial Pearson correlation controlling for age and cognitive score (ACE-R).

To identify potential neurophysiological biomarkers distinguishing PD-SH from PD-CN, we implemented a two-step machine learning pipeline combining supervised classification and feature ranking. Due to the small sample size, we employed a leave-one-out cross-validation (LOOCV) framework across five classifiers using Python Scikit-learn packages (scikit-learn v1.4). The dataset included brain states and significant synergy and redundancy features from individual patients (PD-CN and PD-SH). The five classifiers used are: Logistic Regression (liblinear solver), linear Support Vector Machine (SVM), Random Forest (100 trees), Gaussian Naïve Bayes, and a Multi-layer Perceptron (MLP; 100 hidden units, max_iter=1000). Model performance was evaluated using LOOCV to mitigate small-sample bias. At each LOOCV iteration, classifiers were trained on all but one sample and tested on the held-out sample[43]. Prediction performance was evaluated using accuracy, area under the ROC curve (AUC), sensitivity (true positive rate), and specificity (true negative rate). Receiver operating characteristic (ROC) and precision-recall curves were generated for each classifier to visualize discriminative performance for PD-CN and PD-SH.

Feature selection was performed using MATLAB's fsrftest algorithm, which ranks features based on univariate F-test scores[60]. This analysis included all DFC brain states and higher-order information-theoretic features (synergy and redundancy). The top 20% of ranked features were retained, and all feature values were z-score normalized prior to training. This two-step pipeline classification followed by feature ranking allowed us to assess both the overall discriminative capacity of the models and the relative importance of individual biomarkers.

## Data availability

The MRI and Behavioral data used in this study, along with the experimental details are available in the OpenfMRI database, can be found here: https://www.openfmri.org/dataset/ds000245/.

## Code availability

All code used in this study is publicly available on GitHub. Scripts for dynamic functional connectivity, brain state analysis, information-theoretic

measures (synergy and redundancy), and classifier-based feature ranking can be accessed at: https://github.com/SnehaRayPanda/PD_DFC_Brain_State_Synergy. Glass brain visualizations were generated using the BrainNet Viewer toolbox (https://www.nitrc.org/projects/bnv).

## Abbreviations

| | |
|---|---|
| PD | Parkinson's disease |
| PD-SH | PD patient with severe hyposmia |
| PD-CN | PD patient with cognitive normal ability |
| HC | Healthy controls |
| Rs-fMRI | Resting state functional magnetic resonance imaging |
| FC | Functional connectivity |
| ICA | Independent component analysis |
| DFC | Dynamic functional connectivity |
| ACE-R | Addenbrooke's Cognitive Examination Revised |
| OSIT | Japanese Odour Stick Identification Test |
| MDS-UPDRS | Movement Disorder Society sponsored revision of the Unified Parkinson's Disease Rating Scale |
| AAL | Anatomical Automatic Labeling |
| LEiDA | leading Eigenvector Dynamics method Analysis. |

Received: 18 March 2025; Accepted: 29 July 2025;
Published online: 13 August 2025

## References

1. Mesholam, R. I., Moberg, P. J., Mahr, R. N. & Doty, R. L. Olfaction in neurodegenerative disease: A meta-analysis of olfactory functioning in Ahlzheimer's and Parkinson's diseases. *Arch. Neurol.* **55**, 84 (1998).
2. Bohnen, N. I., Gedela, S., Herath, P., Constantine, G. M. & Moore, R. Y. Selective hyposmia in Parkinson's disease: Association with hippocampal dopamine activity. *Neurosci. Lett.* **447**, 12–16 (2008).
3. Hasan, S. et al. Olfactory dysfunction in incidental Lewy body disease and Parkinson's disease: An update. *Innov. Clin. Neurosci.* **19**, 19–27 (2022).
4. Morley, J. F. et al. Olfactory dysfunction is associated with neuropsychiatric manifestations in Parkinson's disease. *Mov. Disord.* **26**, 2051–2057 (2011).
5. Fagundo, A. B. et al. Modulation of higher-order olfaction components on executive functions in humans. *PLoS One* **10**, e0130319 (2015).
6. Zhou, G., Lane, G., Cooper, S. L., Kahnt, T. & Zelano, C. Characterizing functional pathways of the human olfactory system. *Elife* **8**, e47177 (2019).
7. Martial, C. et al. From nose to brain: The effect of lemon inhalation observed by whole brain voxel to voxel functional connectivity. *Cortex* **165**, 119–128 (2023).
8. Yoneyama, N. et al. Severe hyposmia and aberrant functional connectivity in cognitively normal Parkinson's disease. *PLoS One* **13**, e0190072 (2018).
9. Wang, Y. Functional covariance connectivity of gray and white matter in olfactory-related brain regions in Parkinson's Disease. *Front. Neurosci.* **16**, 853061 (2022).
10. Crimaldi, J. et al. Active sensing in a dynamic olfactory world. *J. Comput. Neurosci.* 50 https://doi.org/10.1007/s10827-021-00798-1 (2022).
11. Bowman, N. E., Kording, K. P. & Gottfried, J. A. Temporal Integration of olfactory perceptual evidence in human Orbitofrontal Cortex. *Neuron* **75**, 916–927 (2012).
12. Hutchison, R. M. et al. Dynamic functional connectivity: Promise, issues, and interpretations. *Neuroimage* **80**, 360–378 (2013).
13. Iravani, B. et al. Acquired olfactory loss alters functional connectivity and morphology. *Sci. Rep.* **11**, 16422 (2021).
14. Hirst, R. J., Setti, A., De Looze, C., Kenny, R. A. & Newell, F. N. Multisensory integration precision is associated with better cognitive performance over time in older adults: A large-scale exploratory study. *Aging Brain* **2**, 100038 (2022).
15. Gatica, M. et al. High-order interdependencies in the aging brain. *Brain Connect.* **11**, 734–744 (2021).
16. Luppi, A. I. et al. A synergistic core for human brain evolution and cognition. *Nat. Neurosci.* **25**, 771–782 (2022).
17. Marinazzo, D. et al. Information transfer and criticality in the ising model on the human connectome. *PLoS One* **9**, e93616 (2014).
18. Timme, N., Alford, W., Flecker, B. & Beggs, J. M. Synergy, redundancy, and multivariate information measures: An experimentalist's perspective. *J. Comput. Neurosci.* **36**, 119–140 (2014).
19. Demertzi, A. et al. Human consciousness is supported by dynamic complex patterns of brain signal coordination. *Sci. Adv.* **5**, eaat7603 (2019).
20. Gibb, W. R. G. Neuropathology of Parkinson's disease and related syndromes. *Neurol. Clin.* **10**, 361–376 (1992).
21. Alonso Martínez, S., Deco, G., Ter Horst, G. J. & Cabral, J. The dynamics of functional brain networks associated with depressive symptoms in a nonclinical sample. *Front. Neural Circuits* **14**, 570583 (2020).
22. Barttfeld, P. et al. Signature of consciousness in the dynamics of resting-state brain activity. *Proc. Natl. Acad. Sci.* **112**, 201418031 (2014).
23. Fiorenzato, E. et al. Dynamic functional connectivity changes associated with dementia in Parkinson's disease. *Brain* **142**, 2860–2872 (2019).
24. Chen, L., Bedard, P., Hallett, M. & Horovitz, S. G. Dynamics of top-down control and motor networks in Parkinson's Disease. *Mov. Disord.* **36**, 916–926 (2021).
25. Gomes, M. T., Fernandes, H. M. & Cabral, J. Deep brain stimulation modulates the dynamics of resting-state networks in patients with Parkinson's Disease. *bioRxiv* at https://doi.org/10.1101/2020.11.04.368274 (2020).
26. Luppi, A. I., Rosas, F. E., Mediano, P. A. M., Menon, D. K. & Stamatakis, E. A. Information decomposition and the informational architecture of the brain. *Trends Cogn. Sci.* v28 https://doi.org/10.1016/j.tics.2023.11.005 (2024).
27. Varley, T. F., Pope, M., Faskowitz, J. & Sporns, O. Multivariate information theory uncovers synergistic subsystems of the human cerebral cortex. *Commun. Biol.* **6**, 451 (2023).
28. Qureshy, A. et al. Functional mapping of human brain in olfactory processing: A PET study. *J. Neurophysiol.* **84**, 1656–1666 (2000).
29. Iannilli, E., Stephan, L., Hummel, T., Reichmann, H. & Haehner, A. Olfactory impairment in Parkinson's disease is a consequence of central nervous system decline. *J. Neurol.* **264**, 1236–1246 (2017).
30. Hoehn, M. M. & Yahr, M. D. Parkinsonism: Onset, progression, and mortality. *Neurology* **17**, 427 (1967).
31. Fazekas, F. et al. The spectrum of age-associated brain abnormalities: Their measurement and histopathological correlates. *J. Neural Transm. Suppl.* (1998), 31-39 https://doi.org/10.1007/978-3-7091-6467-9_4.
32. Saito, S. et al. Development of a smell identification test using a novel stick-type odor presentation kit. *Chem. Senses* **31**, 379–391 (2006).
33. Mioshi, E., Dawson, K., Mitchell, J., Arnold, R. & Hodges, J. R. The Addenbrooke's Cognitive Examination revised (ACE-R): A brief cognitive test battery for dementia screening. *Int. J. Geriatr. Psychiatry* **21**, 1078–1085 (2006).
34. Mccolgan, P. et al. Addenbrooke's Cognitive Examination-Revised for mild cognitive impairment in Parkinson's disease. *Mov. Disord.* **27**, 1173–1177 (2012).
35. Kashihara, K. et al. Official Japanese Version of the International Parkinson and Movement Disorder Society–Unified Parkinson's Disease Rating Scale: Validation Against the Original English Version. *Mov. Disord. Clin. Pract.* **1**, 200–212 (2014).

36. Salimi-Khorshidi, G. et al. Automatic denoising of functional MRI data: Combining independent component analysis and hierarchical fusion of classifiers. *Neuroimage* **90**, 449–468 (2014).
37. Pruim, R. H. R. et al. ICA-AROMA: A robust ICA-based strategy for removing motion artifacts from fMRI data. *Neuroimage* **112**, 267–277 (2015).
38. Griffanti, L. et al. Hand classification of fMRI ICA noise components. *Neuroimage* **154**, 188–205 (2017).
39. Murphy, K., Birn, R. M., Handwerker, D. A., Jones, T. B. & Bandettini, P. A. The impact of global signal regression on resting state correlations: Are anti-correlated networks introduced?. *Neuroimage* **44**, 893–905 (2009).
40. Hahamy, A. et al. Save the global: global signal connectivity as a tool for studying clinical populations with functional magnetic resonance imaging. *Brain Connect.* **4**, 395–403 (2014).
41. Li, J. et al. Topography and behavioral relevance of the global signal in the human brain. *Sci. Rep.* **9**, 14286 (2019).
42. Rolls, E. T., Joliot, M. & Tzourio-Mazoyer, N. Implementation of a new parcellation of the orbitofrontal cortex in the automated anatomical labeling atlas. *Neuroimage* **122**, 1–5 (2015).
43. Finn, E. S. et al. Functional connectome fingerprinting: identifying individuals using patterns of brain connectivity. *Nat. Neurosci.* **18**, 1664–1671 (2015).
44. Smith, S. M. et al. Advances in functional and structural MR image analysis and implementation as FSL. *NeuroImage* **23**, S208–S219 (2004).
45. Panda, R. et al. Posterior integration and thalamo-frontotemporal broadcasting are impaired in disorders of consciousness. *Hum. Brain Mapping, Press* https://doi.org/10.1101/2021.11.08.467694 (2023).
46. Engels, G., Vlaar, A., McCoy, B., Scherder, E. & Douw, L. Dynamic functional connectivity and symptoms of Parkinson's Disease: A resting-state fMRI study. *Front. Aging Neurosci* **10**, 388 (2018).
47. Filippi, M., Sarasso, E. & Agosta, F. Resting-state Functional MRI in Parkinsonian Syndromes. *Movement Disord. Clin. Pract*. **6** https://doi.org/10.1002/mdc3.12730 (2019).
48. Lenka, A. et al. Freezing of gait in Parkinson's disease is associated with altered functional brain connectivity. *Park. Relat. Disord. J.* **24**, 100–106 (2016).
49. Glerean, E., Salmi, J., Lahnakoski, J. M., Jääskeläinen, I. P. & Sams, M. Functional magnetic resonance imaging phase synchronization as a measure of dynamic functional connectivity. *Brain Connect.* **2**, 91–101 (2012).
50. Deco, G., Kringelbach, M. L., Jirsa, V. K. & Ritter, P. The dynamics of resting fluctuations in the brain: Metastability and its dynamical cortical core. *Sci. Rep.* **7**, 3095 (2017).
51. Panda, R. et al. Disruption in structural-functional network repertoire and time resolved subcortical-frontoparietal connectivity in disorders of consciousness. *BioRxiv* https://doi.org/10.1101/2021.12.10.472068 (2021).
52. López-González, A. et al. Loss of consciousness reduces the stability of brain hubs and the heterogeneity of brain dynamics. *Commun. Biol.* **4**, 2020.11.20.391482 (2021).
53. Cabral, J. et al. Cognitive performance in healthy older adults relates to spontaneous switching between states of functional connectivity during rest. *Sci. Rep.* **7**, 5135 (2017).
54. Lord, L. D. et al. Dynamical exploration of the repertoire of brain networks at rest is modulated by psilocybin. *Neuroimage* **199**, 127–142 (2019).
55. Acharya, U. V. et al. Functional network connectivity imprint in febrile seizures. *Sci. Rep.* **12**, 3267 (2022).
56. Rubinov, M. & Sporns, O. Complex network measures of brain connectivity: Uses and interpretations. *Neuroimage* **52**, 1059–1069 (2010).
57. Hutchison, R. M. & Morton, J. B. Tracking the brain's functional coupling dynamics over development. *J. Neurosci.* **35**, 6849–6859 (2015).
58. Panda, R. et al. Disruption in structural–functional network repertoire and time-resolved subcortical fronto-temporoparietal connectivity in disorders of consciousness. *Elife* **11**, e77462 (2022).
59. Lizier, J. T. Measuring the dynamics of information processing on a local scale in time and space. *Understand. Complex Syst.* at https://doi.org/10.1007/978-3-642-54474-3_7 (2014), 161-193.
60. Avots, E. et al. Ensemble approach for detection of depression using EEG features. *Entropy* **24**, 211 (2022).


## Acknowledgements

We are thankful to Yoneyama et al.[8] for providing the MRI and Behavioral data and experimental details in the OpenfMRI database. We extend our sincere thanks to Prof. Ris Laurence from the Department of Neuroscience, Université de Mons, Belgium, for her guidance and support throughout this research.

## Author contributions

Sneha Ray, Neeraj Upadhyay, Rajanikant Panda designed research. Neeraj Upadhyay and Henning Boecker supervised the research. Sneha Ray selected the data from an open database, preprocessed and analyzed the data. Rajanikant Panda guided in optimizing the code as per this research study and supervised the methods used. Sneha Ray, Neeraj Upadhyay, Rajanikant Panda wrote the manuscript. Henning Boecker, Navkiran Kalsi and Neeraj Upadhyay gave the critical comments and suggestions of result interpretation and manuscript review. All authors interpreted the results and contributed to the editing/reviewing of the manuscript.

## Competing interests

The authors declare no competing interests.

## Additional information

**Correspondence** and requests for materials should be addressed to Rajanikant Panda.